CrystEngComm

PAPER

View Article Online
View Journal | View Issue

Cite this: *CrystEngComm*, 2025, **27**, 5743

Understanding the relationship between the crystal structure elastic–plastic properties of discrete-molecule organic–inorganic halide perovskites†

Jacob L. Hempel,[a] Michael D. Wells,[c] Sean Parkin,[c] Yang-Tse Cheng[ab] and Aron J. Huckaba *[c]

Discrete-molecule hybrid perovskites with different organic and inorganic molecules can provide a wide array of tunable optoelectronic and piezoelectronic properties. In this study, we report the elastic modulus and hardness, obtained from instrumented indentation measurements, of three new and three known discrete-molecule single crystal halide metalates, with an aim towards understanding the relationship between their microstructure and mechanical properties. We find a correlation in the mechanical properties and the density of the crystal structure, as well as with the number of hydrogen bonding sites available on the organic cation. These two observations suggest that denser crystal structures with more hydrogen bonding sites lead to stronger intermolecular interactions, thereby increasing the elastic modulus. Contrary to previous findings in the literature, we also find that the metal–halide bond strength does not significantly influence the elastic modulus in this set of data. We rationalize this observation by the differences in supramolecular network dimensionality between the literature reports and the crystals presented in this study, thus concluding that the metal–halide bond strength plays an insignificant role in determining the elasticity of discrete-molecule single crystal hybrid perovskites.

Received 17th July 2025,
Accepted 25th July 2025

DOI: 10.1039/d5ce00716j

rsc.li/crystengcomm

1. Introduction

Organic–inorganic halide metallates (OIHMs) are materials with the general formula $A_m^{x+}B^{n+}X_{(m*x)+n}$, where A denotes a cation (either organic, like $H_3CNH_3^+$ or inorganic, like Cs^+), B denotes a metal cation (often doubly cationic), and X denotes an anion like Cl^-, Br^-, or I^-.[1] Interest in these materials has grown recently due to their large absorption coefficients,[2] long charge-carrier diffusion lengths,[3] and easily tunable bandgaps.[4] They are quickly nearing commercial application, especially in photovoltaics, where power-conversion efficiencies have exceeded 30% in Si-perovskite tandem devices.[5] By varying the A, B, and X ions the degree of halide sharing can be controlled.[6] Total halide sharing yields 3D-network halide perovskites, while lesser degrees of halide sharing gives layered, catemeric, and discrete-molecule (commonly, but incorrectly 2D, 1D, 0D, respectively) halometallates, which deviate from the classic perovskite structure. While optoelectronic properties of these materials are a clear motivator for research in using these materials for applications, understanding the mechanical properties of these materials is vital in bringing the materials from the lab into real world applications, where they are required to bend, stretch, and/or flex.[7]

One field of research where the mechanical properties of OIHMs play a pivotal role is in piezoelectric applications. When OIHMs crystallize with noncentrosymmetric space group symmetry, they exhibit piezoelectric properties that can be used to extract energy from ambient mechanical vibrations. In the field of piezoelectric energy harvesting, we find many applications converting ambient mechanical stresses and strains into useable electrical power, including harvesting energy from roadway traffic and railways,[8–12] from wind and waterflow,[13–19] and from movement of the human body.[20–23] Many of the devices made for these applications use geometries in which knowing the elastic modulus of both active and passive materials is paramount for designing devices that have large power outputs.[24] The elastic modulus and Poisson's ratio of piezoelectric OIHMs are needed for the coupled piezoelectric-circuit finite-element model, which can

[a] *Department of Physics and Astronomy, University of Kentucky, Lexington, KY 40506, USA*
[b] *Department of Chemical and Materials Engineering, University of Kentucky, Lexington, KY 40506, USA*
[c] *Department of Chemistry, University of Kentucky, Lexington, KY 40506, USA. E-mail: aron.huckaba@uky.edu*

† Electronic supplementary information (ESI) available. CCDC 2383154 and 2383155. For ESI and crystallographic data in CIF or other electronic format see DOI: https://doi.org/10.1039/d5ce00716j

be used to model the power output of piezoelectric devices.[25] It is thus important to understand the relationship between the chemistry and structure of these materials and their elastic properties in order to help future engineers find the ideal materials for a particular application.

There are some studies that have been conducted on the elastic modulus of OIHP materials aiming to find connections between the chemistry and microstructure of the perovskite and their elastic properties by performing nanoindentation experiments relative to different crystallographic axes or by changing the inorganic component of the crystal structure. Sun *et al.* found that the elastic modulus for $CH_3NH_3PbX_3$ (X = I, Br, and Cl), which has a triperiodic network, depended on X and was slightly anisotropic, whilst also finding correlations between the metal–halide bond strengths, electronegativity, and tolerance factors with the Young's modulus.[26] The result that the modulus depends upon the metal–halide bond strengths agrees well with the common intuition that bond strength in solids is proportional to their modulus of elasticity. This intuition is further backed by considering the potential energy, U, of two atoms separated by some equilibrium distance r_0. One finds that the elastic modulus, $E = S_0/r_0$, where S_0 is the second derivative of the potential energy, $S_0 = d^2U/dr^2$. Rakita *et al.* also compared the elastic moduli of triperiodic $APbX_3$ (A = Cs, CH_3NH_3, X = I, Br) OIHMs with theoretically calculated values and classified OIHMs based on their mechanical properties.[27] They found that the average Pb–X bond distance was inversely proportional to the measured bulk modulus from nanoindentation experiments, which agrees well with the discussion above.

As the periodicity of the metal–halide bonded module decreases from 3 to 2, there is a lower degree of halide sharing between metal centers, resulting in more anisotropic elastic behavior. Usually these materials are layered, in the sense that the halide-sharing inorganic metal tetrahedra form sheets that are separated by organic layers. The anisotropy in this system has been demonstrated in a nanoindentation and DFT study on the diperiodic layered lead halide hybrid, $(C_6H_5CH_2NH_3)PbCl_4$ by Wei *et al.*, which showed that the anisotropy in the calculated elastic modulus from DFT calculations increases as the relative number of the inorganic to organic layers decreases.[29] Their calculations also suggest that the ductility of this material is a function of the number of inorganic layers present. Since the organic layers in these materials mostly interact *via* van der Waals and hydrogen bonding, which are weaker than covalent bonds. It is also expected that the modulus would be inversely proportional to the relative proportion of organic to inorganic layers. This has been found in a study by Tu *et al.*, which looked at the mechanical properties of diperiodic layered OIHMs using nanoindentation and found that the elastic modulus decreased as the inorganic layers were separated by larger organic layers.[28] Elastic anisotropy has also been found in mono-periodic (*i.e.*, catemeric) OIHMs. A study by Wei *et al.* performed indentation measurements on a catemeric hybrid lead iodide single crystal specimen and found that the measured elasticity depended on the relative orientation between the indentation axis and the axis of the metal inorganic chains.[29]

Discrete-molecule OIHMs have no degree of halide sharing, thus intermolecular forces such as hydrogen bonding, van der Waals forces, and π–π stacking are ultimately what determine their stiffnesses. Such systems are commonly found in organic molecular crystals such as saccharin[30] and aspirin.[31] These crystals typically exhibit interesting and counterintuitive mechanical behavior such as high mechanical flexibility[32] and large ferroelasticity,[33,34] which drove the field to develop a mechanistic understanding of their properties and to find relationships between structure and elasticity. It was found that the strength and topology of hydrogen bonding within the molecular crystal is an important factor that determines the strength and anisotropy of the elastic modulus of single crystal specimens.[35]

The main questions that this indentation study aims to answer are as follows:

1. How does the elastic modulus of discrete-molecule OIHMs depend upon the choice of the organic cation?

2. How does the modulus depend upon the metal–halide bond strength?

Nanoindentation is a well-suited tool for investigating questions such as these because it measures the elasticity of small volumes of material, such as single crystals. We performed indentation measurements and XRD on six different single crystal discrete-molecule OIHM samples and report the relationship between their elastic moduli and structure. To study the metal–halide bond strength, we compare the elastic moduli of histammonium $ZnCl_4$ (HistZn) with histammonium $CoCl_4$ (HistCo). We then compare these results with indentation measurements on 1-methylimidazolium $ZnCl_4$ (MIZn), (1,3) dimethylimidazolium $ZnCl_4$ (DMIZn), 1-butyl pyridinium$_2ZnCl_4$ (1BPmZn), and 1-butyl-1-methyl pyrollidinium $ZnCl_4$ (1B1MPyZn) to study the effect the choice of organic cation has on the measured moduli. Finally, we draw comparisons between the different families of materials and their crystal structures with the aim of determining what structural properties influence the elasticity of samples the most and relate these conclusions to published literature discussed above.

2. Methods

2.1. Materials

All chemicals used were acquired from commercial suppliers and used as received with no further preparation. $ZnCl_2$ (VWR); $CoCl_2{\cdot}6H_2O$ (VWR); tetramethylammonium chloride (>98.0%, TCI); trimethylammonium chloride (>97.0%,TCI); 1-butyl-1-methylpyrrolidinium chloride (>98.0%, TCI); 1-butylpyridinium chloride (>98.0%, TCI); methanol (VWR); reagent alcohol (95%, VWR); hydrochloric acid (36.5–38%, VWR); diethyl ether (VWR).

2.2. Preparation of the metallates

1-Butyl-1-methylpyrrolidinium and 1-butylpyrridinium metalates were prepared using 5 mL solutions of 90% reagent ethyl

alcohol and 10% of an aqueous 5% HCl solution in 1 dram vials. Hydrochloride salts of the organic cations were mixed with anhydrous $ZnCl_2$ or $CoCl_2{\cdot}6H_2O$ in ratios of two (2) organic cation equivalents to one (1) of metal halide to achieve the appropriate stoichiometry, *i.e.* A_2MX_4. With A representing the cationic amine, M as the metal of choice, and X the halide component; chlorine in this case. Metal halides were used at 7.5 mmol, 1.5 M concentration.

Each vial was warmed to 60 °C to dissolve the contents, then kept at that temperature to encourage slow crystal growth. All samples were monitored by eye for crystal growth and those that produced no solids were dropped in temperature by 5-degree decrements every 24 hours until crystal growth was observed. Small crystals that grew were removed, their growth solution re-heated to dissolve the contents and the seed crystal re-introduced at the temperature at which they grew until uniform crystals of a suitable size were achieved.

Those samples that dissolved poorly or not at all at elevated temperatures were charged with additional DI water in 0.5 mL increments until full dissolution of the solids. The growth time required for crystals of suitable size varied from species to species, ranging from 24 hours to 2 weeks or more. Crystal samples such as 1B1MPyZn and 1BPmZn, which did not grow seed crystals even at room temperature, were refrigerated as necessary to promote growth and the same seeding process used.

The 1B1MPyZn species gave few seed crystals of acceptable quality until the solvent was removed by evaporation and the remnant solids were dissolved in a minimal amount of 100% methanol. Performing a vapor-diffusion crystallization against diethyl ether as an antisolvent yielded suitable characterization specimens within 24 hours.

2.3. Characterization

All single crystal data was either available from the Cambridge Crystallographic Data Centre (CCDC) or collected on a Bruker D8 Venture dual-microsource κ-axis diffractometer with large-area 'Photon' CMOS detector equipped with a low-temperature device at 90.0 K. The radiation source was Mo Kα (0.71073 Å). Structures were solved by dual-space methods and refined by full-matrix least-squares on F^2 using the Shelx programs. Even though both 1-butyl-1-methylpyrrolidinium and 1-butyl pyridinium$_2ZnCl_4$ single crystals were grown, they were not suitable for single crystal XRD.

Instrumented indentation was employed to determine the elastic modulus of single crystal samples (Fig. 1). Single crystal specimens were first mounted onto small glass 2.5 × 2.5 cm squares using a stereomicroscope, an acupuncture needle, and 5 minute epoxy (JB Clear Weld). The glass squares were then epoxied onto pucks and transferred to a G200 Agilent Nano Indenter that was housed within an argon-filled glovebox. All indentation measurements took place under dry conditions inside the glovebox with <0.1 PPM H_2O/O_2. Depth-controlled indentation measurements were performed down to 2 μm with a constant target strain-rate of 0.05 s^{-1} with a diamond

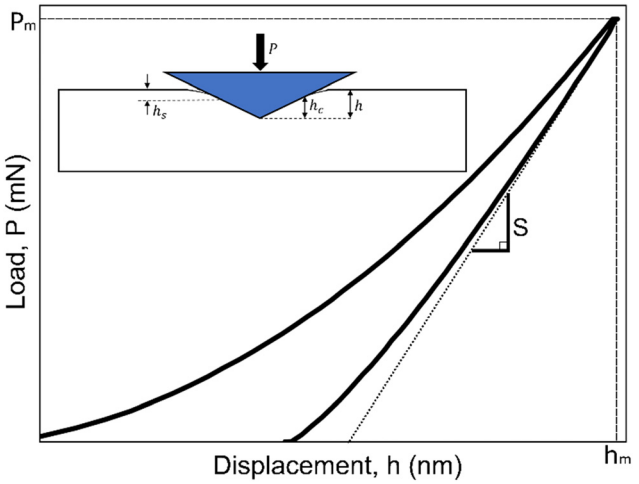

Fig. 1 Example of a load–displacement curve obtained from an indentation experiment. Inset shows a physical picture of a sharp indenter being pressed into a sample. Note that this picture shows material sinking in around the tip rather than piling up.

Berkovich tip. The tip was held at the maximum displacement for 15 seconds before unloading to remove any potential rate-dependent plastic deformation from influencing the modulus and hardness measurement. The reduced modulus was calculated from the slope of the unloading curve at the maximum load, S:

$$E_r = \frac{S(h_c)\sqrt{\pi}}{2\beta\sqrt{A(h_c)}} \quad (1)$$

where β is a geometric constant determined by the geometry of the indenter (β = 1.024 for a Berkovich tip) and $A(h_c)$ is the projected contact area of the tip at contact depth at maximum load, h_c, which is obtained using the Oliver–Pharr method:[36]

$$h_c = h - \varepsilon\frac{P_m}{S} \quad (2)$$

where ε is a geometric constant (ε = 0.72 for a Berkovich tip).

The hardness is determined by dividing the max load, P_m, by the contact area at the contact depth:

$$H = \frac{P_m}{A(h_c)} \quad (3)$$

Indentation was performed on two to three separate single crystal specimens at different spots across the crystal surface. Three spots, each containing 5 indents, were chosen for each crystal to determine how the modulus may vary across the crystal. The validity of this methodology was verified on two small crystals of 99% pure NaCl salt purchased from Sigma Aldrich and showed excellent agreement with literature values (see Fig. S1†).

3. Results and discussion

Fig. 2 shows the load-depth curves for every compound in this study. The data in each of the plots includes data from

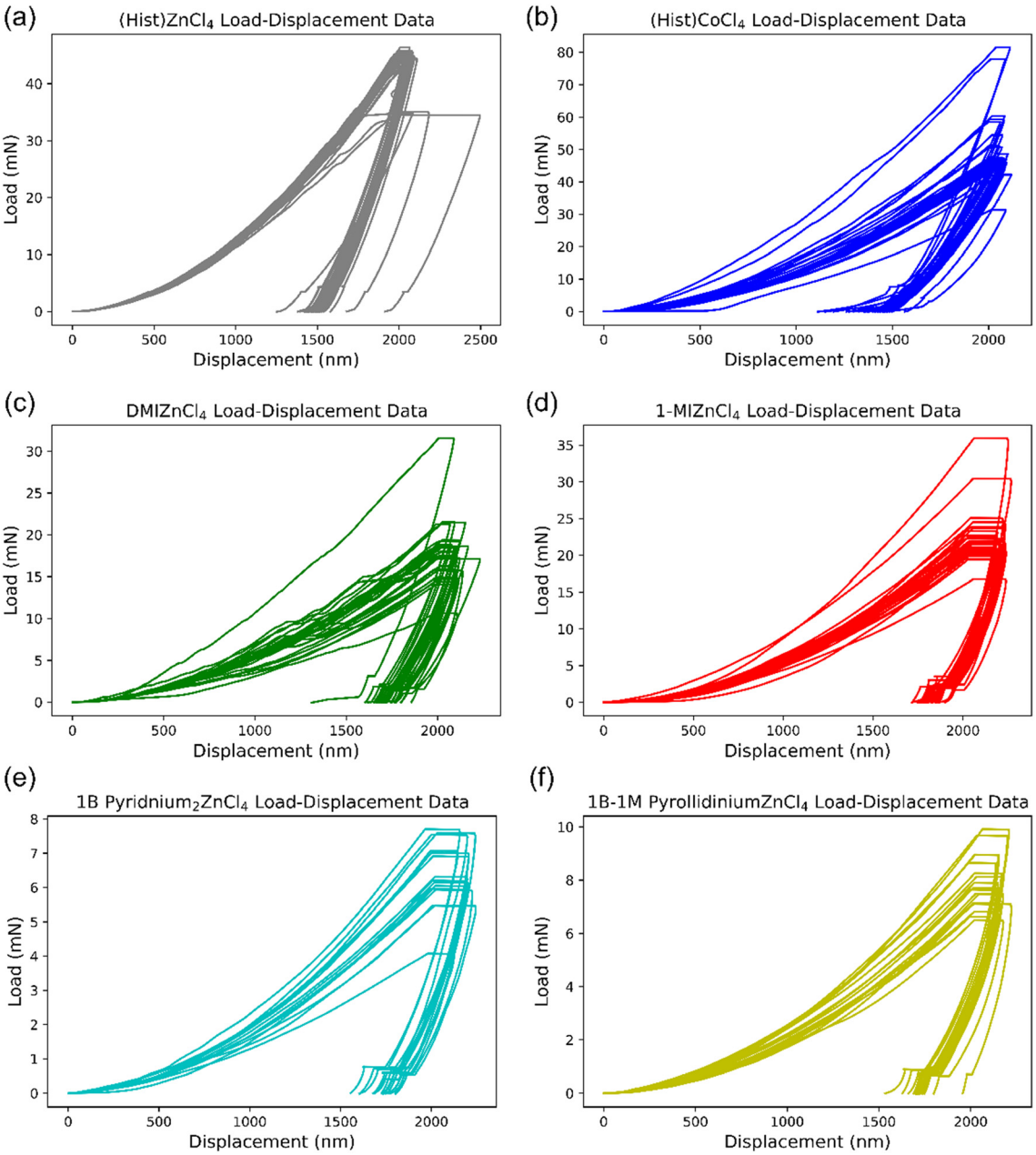

Fig. 2 Load–displacement curves of all indents from all crystals in this study: (a) histammonium $ZnCl_4$ (b) histammonium $CoCl_4$, (c) (1,3) dimethylimidazolium $ZnCl_4$, (d) 1-methylimidazolium $ZnCl_4$, (e) 1-butyl pyridinium$_2ZnCl_4$, and (f) 1-butyl-1-methyl pyrollidinium $ZnCl_4$.

all two or three crystals that were measured. Note the differences in scale along the *y*-axis. 1BPyZn and 1B1MPmZn required significantly lower force to reach the same depth of indentation, resulting in a lower average hardness, as reported in Table 1. These two compounds also show a significantly lower elastic modulus compared to the others

Table 1 Summary of the average modulus and hardness obtained from the indentation study along with the density as obtained from the solved crystal structure

Crystal	Elastic modulus (GPa)	Hardness (GPa)	Density (g cm^{-3})
(Hist)$ZnCl_4$ (HZn)	10.70 ± 1.09	0.48 ± 0.05	1.813
(Hist)$CoCl_4$ (HCo)	11.19 ± 1.61	0.53 ± 0.11	1.775
Dimethylimidazolium $ZnCl_4$ (DMIZn)	6.78 ± 1.11	0.17 ± 0.04	1.568
1-Methylimidazolium $ZnCl_4$ (MIZn)	9.83 ± 1.73	0.18 ± 0.03	1.677
1-Butyl-pyridinium $ZnCl_4$ (1BPmZn)	1.99 ± 0.24	0.05 ± 0.01	N/A
1-Butyl-1-methyl-pyrollidinium $ZnCl_4$ (1B1MPyZn)	1.09 ± 0.07	0.07 ± 0.01	N/A

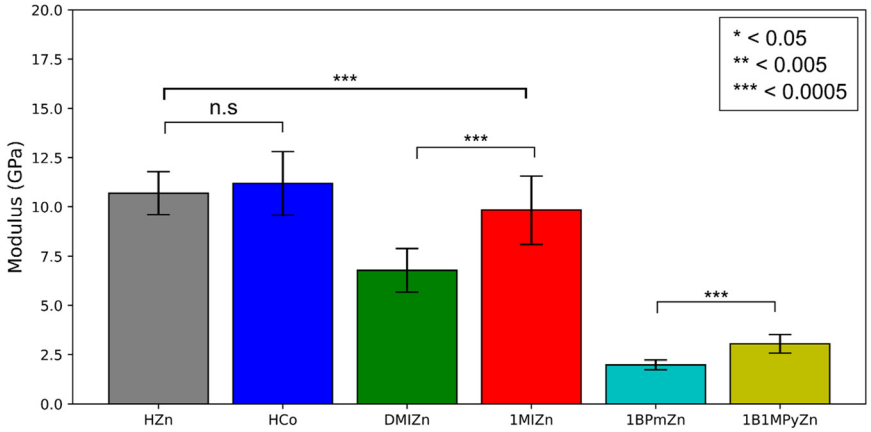

Fig. 3 Summary of the measured elastic moduli for every compound presented in this study along with relevant statistical *t*-tests which compared certain compound averages.

and were the most difficult samples to crystallize and characterize with XRD. The fact that the crystals were difficult to crystallize lends credence to the idea that the intermolecular forces in 1BPyZn and 1B1MPmZn are significantly weaker than the other samples, which also leads to the materials having a lower elastic modulus. We also observe that the loading curves in $DMIZnCl_4$ shown in Fig. 2c contain pop-in events. Pop-in events have been previously observed in other hybrid organic–inorganic perovskites. Reyes-Martinez attributed the first pop-in event to the onset of plastic deformation in their report on Cs-based perovskites.[37] Other reports attribute these events to the breaking of hydrogen bonds.[38,39] The latter attribution may be possible in our results, given that dimethylimidazolium does not contain many suitable hydrogen bonding sites, as will be discussed later, making the intermolecular interactions from hydrogen bonding for this crystal substantially weaker than the case of methylimidazolium and histammonium, which contain one and three nitrogen–hydrogen pairs that act as hydrogen bond donor sites. There was no clear indication of cracking in DMIZn (see the Fig. S4†), but pop-in events have also been attributed to fracturing, especially chipping.

Fig. 3 presents a comparison of the elastic modulus for all materials presented here. A Student's *t*-test was performed to compare the average modulus of HZn with HCo, where it was found that they do not differ significantly. This is interesting because the Cl–Co bond has an enthalpy of formation of ΔH_f = 398 kj mol^{-1} while the Cl–Zn bond has ΔH_f = 229 kj mol^{-1}.[40] One would therefore expect that HCo to have a higher modulus than HZn since the bond strength is higher. This result can be explained by the fact that the crystals are non-periodic discrete molecules, leading to a lack of long-range order for the metal–halide bonds. When the ligands are shared, as is the case for $CH_3NH_3PbX_3$,[26] the bond strength between the metal center and the halogen atom will play a more prominent role in the elastic deformation of the crystal since large scale deformations relative to the unit cell would include significantly more halide–metal interactions.

We also compared the average moduli of DMIZn and 1MIZn and found that the two moduli differ with statistical significance ($p < 0.05$), where 1MIZn was found to be larger than DMIZn. This can be rationalized by comparing the chemical structure of (1,3)

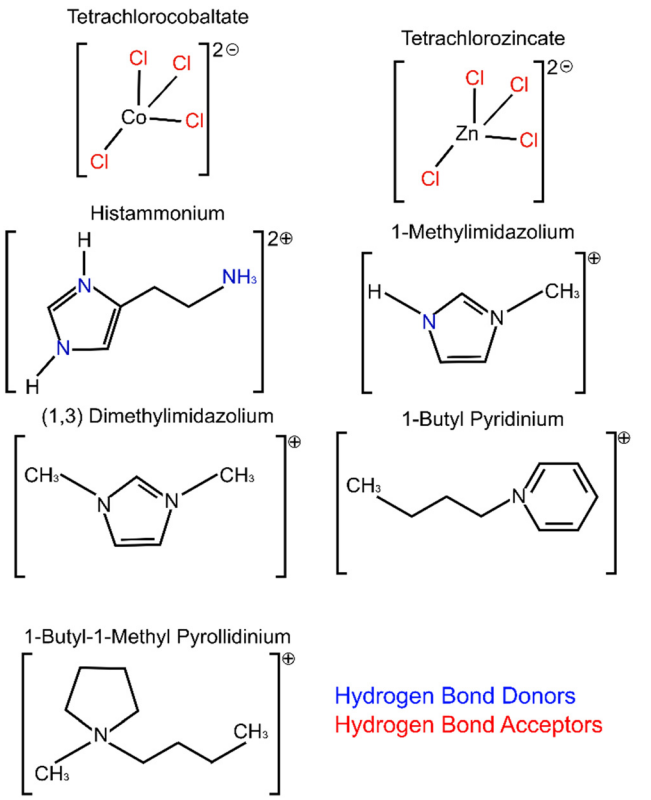

Fig. 4 Chemical structure for all the different inorganic and organic components in the single crystal samples.

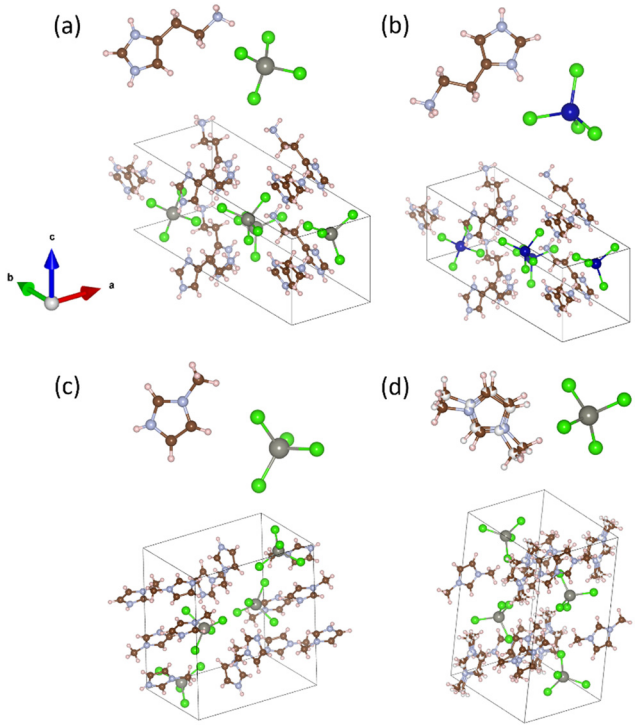

Fig. 5 Solved crystal structure as obtained from crystal XRD for (a) histammonium $ZnCl_4$, (b) histammonium $CoCl_4$, (c) 1-methylimidazolium $ZnCl_4$, and (d) (1,3)dimethylimidazolium $ZnCl_4$.

dimethylimidazolium (DMI) with 1-methylimidazolium (1-MI) (Fig. 4). Since the methyl groups are bonded to the nitrogen atoms in the imidazole, there are no hydrogen bonding donor sites available on the organic cation. This results in an overall decrease in the interaction strength between the organic and inorganic parts of the crystal structure, leading to a lower elastic modulus. 1-MI has a single nitrogen atom taken by a methyl group, leaving the other nitrogen free to act as a hydrogen bond donor. The result is a crystal structure that is stiffer when the organic cations crystallize with tetrachlorozincate, as it contains several hydrogen bond acceptor sites. Evidence for this hypothesis is further corroborated when comparing HZn with MIZn. The average modulus for MIZn is measured to be statistically significantly lower than HZn. This can be explained by noting that HZn contains two more hydrogen bond donor sites than MIZn, since both the lone nitrogen in the imidazole and the ammonium in the histammonium organic cation can also participate in hydrogen bonding. The distance of these hydrogen bond interactions (N–Cl) is measured at 3.295 Å and 3.269 Å, the lengths of which indicate a relatively longer H-bond and longer than was found for HZn and HCo (3.129 Å and 3.206 Å).

The elastic modulus of the crystals containing 1-butyl pyridinium (1BPm) is found to be lower than 1-butyl-1-methyl pyrrolidinium (1B1MPy), despite both organic cations containing no hydrogen bond donor sites, while both samples were found to have the lowest elastic modulus in the entire data set, likely due, in part, to the lack of hydrogen bonding sites. 1BPm contains 3 double bonds in its aromatic carbon ring whereas 1B1MPy contains neither double bonds nor aromatic rings. As such, the net intermolecular π–π interactions present between the 1BPm cations is expected to be higher than that of 1B1MPy. Since we find that the elastic modulus of 1B1MPy is higher than 1-butyl pyridinium, we conclude instead that the van der Waals interactions of the 1B1MPy must play a larger role in determining the elasticity when comparing these two cases than does the π–π (interactions).

The solved crystal structures are presented in Fig. 5. We were unable to obtain the structures for 1BPmZn and 1B1MPyZn due to issues with crystal quality. The two

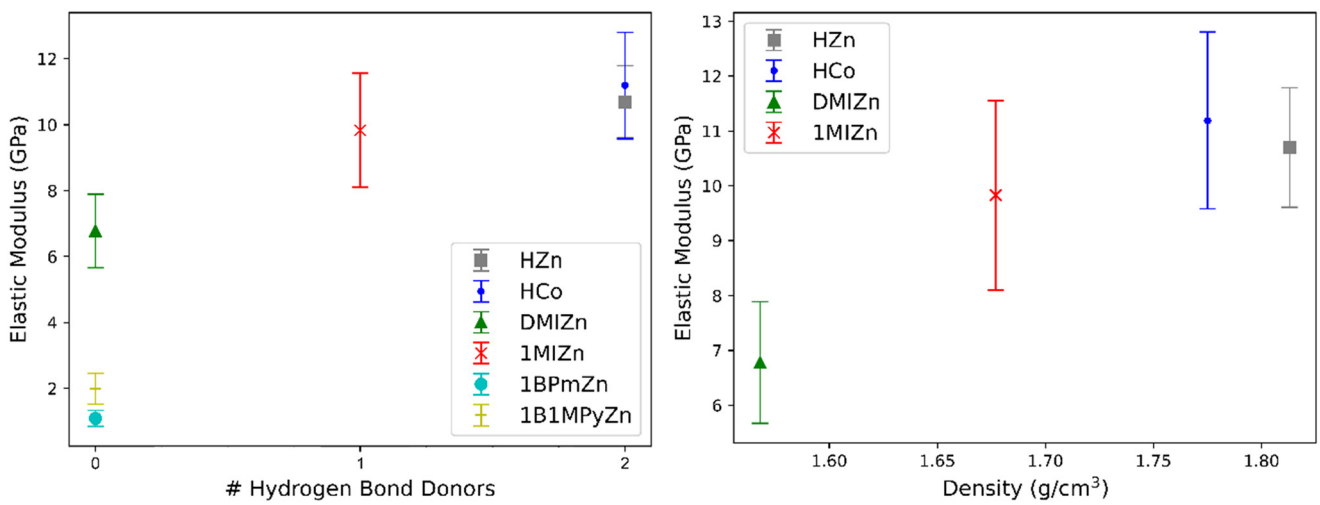

Fig. 6 (left) Relationship between the elastic modulus and number of hydrogen bonding donor sites present on the organic cation. (right) A comparison of the modulus and density of each crystal as obtained from XRD measurements.

superimposed organic cations shown in Fig. 5d for DMIZn indicate that the crystal contained orientational disorder, meaning that some percentage of unit cells contained DMI cations in one orientation while the rest contained cations in a second orientation. This disorder along with the fact that 1BPmZn and 1B1MPyZn structures could not be satisfactorily resolved may also be explained in part by poor intermolecular interaction strength between the cations and anions due to a lack of hydrogen bonding, which tracks with the measurements of their elastic moduli.

The theoretical densities calculated from the crystal structure, elastic moduli, and hardness values of each compound are listed in Table 1. For organic crystals, a correlation was found between the elastic modulus and density.[41] This makes sense given that a higher density would imply that the average equilibrium distance between molecules would be lower. As discussed in the introduction, this is known to be inversely proportional to the elastic modulus, hence a higher density leads to a higher modulus. Fig. 6 shows a plot of the density *versus* elastic modulus for all crystals in this study. We find a correlation between the modulus and the density, which agrees well with the established view that density is proportional to elastic modulus. Also plotted in Fig. 6 is the relationship between the number of hydrogen bond donors in the organic cation and the elastic modulus. While the trend is generally upwards, when there are no hydrogen bond donors in the organic cation, the relationship is less clear.

4. Conclusions

We have established a relationship between the elastic modulus of single crystal hybrid discrete-molecule chlorometallate crystals with their crystal structures. Among the six different crystalline materials, the elastic modulus and hardness of five of them have not been previously reported. We found that the elastic modulus of such structures seems to depend mostly on intermolecular forces and less on intramolecular forces, due to the lack of long-range order in covalent bonding. Specifically, we determined that using organic cations containing possible hydrogen bonding sites leads to crystals with higher elasticity. We did not find any trends in the resulting hardness values, except that denser crystals tend to be harder. These results should provide better insight into the ways crystal engineers fine tune the mechanical properties of hybrid halide–metallate crystals for future applications.

Data availability

The data supporting this article have been included as part of the ESI.† CCDC 2383154 and 2383155 contain the supplementary crystallographic data for this paper.

Conflicts of interest

There are no conflicts to declare.

Acknowledgements

This material is based upon work supported by the National Science Foundation under Cooperative Agreement No. 1849213. AH would like to acknowledge funding from the Eppley Foundation.

References

1 A. K. Jena, A. Kulkarni and T. Miyasaka, Halide perovskite photovoltaics: background, status, and future prospects, *Chem. Rev.*, 2019, **119**(5), 3036–3103, DOI: **10.1021/acs.chemrev.8b00539**.
2 Z. Chen, Q. Dong, Y. Liu, C. Bao, Y. Fang and Y. Lin, *et al.*, Thin single crystal perovskite solar cells to harvest below-bandgap light absorption, *Nat. Commun.*, 2017, **8**(1), 1890, DOI: **10.1038/s41467-017-02039-5**.
3 C. Wehrenfennig, G. E. Eperon, M. B. Johnston, H. J. Snaith and L. M. Herz, High charge carrier mobilities and lifetimes in organolead trihalide perovskites, *Adv. Mater.*, 2014, **26**(10), 1584, DOI: **10.1002/adma.201305172**.
4 G. E. Eperon, S. D. Stranks, C. Menelaou, M. B. Johnston, L. M. Herz and H. J. Snaith, Formamidinium lead trihalide: a broadly tunable perovskite for efficient planar heterojunction solar cells, *Energy Environ. Sci.*, 2014, **7**(3), 982–988, DOI: **10.1039/C3EE43822H**.
5 M. Jost, E. Köhnen, A. Al-Ashouri, T. Bertram, T. Sp and A. Magomedov, *et al.*, Perovskite/CIGS tandem solar cells: from certified 24.2% toward 30% and beyond, *ACS Energy Lett.*, 2022, **7**(4), 1298–1307, DOI: **10.1021/acsenergylett.2c00274**.
6 Q. A. Akkerman and L. Manna, What defines a halide perovskite?, *ACS Energy Lett.*, 2020, **5**(2), 604–610, DOI: **10.1021/acsenergylett.0c00039**.
7 F. Di Giacomo, A. Fakharuddin, R. Jose and T. M. Brown, Progress, challenges and perspectives in flexible perovskite solar cells, *Energy Environ. Sci.*, 2016, **9**(10), 3007–3035, DOI: **10.1039/C6EE01137C**.
8 N. Bosso, M. Magelli and N. Zampieri, Application of low-power energy harvesting solutions in the railway field: a review, *Veh. Syst. Dyn.*, 2021, **59**(6), 841–871, DOI: **10.1080/00423114.2020.1726973**.
9 M. Gao, P. Wang, Y. Cao, R. Chen and C. Liu, A rail-borne piezoelectric transducer for energy harvesting of railway vibration, *J. Vibroengineering*, 2016, **18**(7), 4647–4663, DOI: **10.21595/jve.2016.16938**.
10 I. Jung, Y.-H. Shin, S. Kim, J.-y. Choi and C.-Y. Kang, Flexible piezoelectric polymer-based energy harvesting system for roadway applications, *Appl. Energy*, 2017, **197**, 222–229, DOI: **10.1016/j.apenergy.2017.04.020**.
11 M. Khalili, A. B. Biten, G. Vishwakarma, S. Ahmed and A. Papagiannakis, Electro-mechanical characterization of a piezoelectric energy harvester, *Appl. Energy*, 2019, **253**, 113585, DOI: **10.1016/j.apenergy.2019.113585**.
12 Y. Song, C. H. Yang, S. K. Hong, S. J. Hwang, J. H. Kim and J. Y. Choi, *et al.*, Road energy harvester designed as a macro-power source using the piezoelectric effect, *Int. J. Hydrogen*

Energy, 2016, **41**(29), 12563–12568, DOI: **10.1016/j.ijhydene.2016.04.149**.

13 Y. Cha, W. Chae, H. Kim, H. Walcott, S. D. Peterson and M. Porfiri, Energy harvesting from a piezoelectric biomimetic fish tail, *Renewable Energy*, 2016, **86**, 449–458, DOI: **10.1016/j.renene.2015.07.077**.

14 Y. Cha, H. Kim and M. Porfiri, Energy harvesting from underwater base excitation of a piezoelectric composite beam, *Smart Mater. Struct.*, 2013, **22**(11), 115026, DOI: **10.1088/0964-1726/22/11/115026**.

15 *Energy Harvesting From Hydraulic Pressure Fluctuations*, ed. K. A. Cunefare, N. Verma, A. Erturk, E. Skow, J. Savor and M. Cacan, Smart Materials, Adaptive Structures and Intelligent Systems, American Society of Mechanical Engineers, 2012, DOI: **10.1115/SMASIS2012-7926**.

16 A. Erturk and G. Delporte, Underwater thrust and power generation using flexible piezoelectric composites: an experimental investigation toward self-powered swimmer-sensor platforms, *Smart Mater. Struct.*, 2011, **20**(12), 125013, DOI: **10.1088/0964-1726/20/12/125013**.

17 S. Orrego, K. Shoele, A. Ruas, K. Doran, B. Caggiano and R. Mittal, *et al.*, Harvesting ambient wind energy with an inverted piezoelectric flag, *Appl. Energy*, 2017, **194**, 212–222, DOI: **10.1016/j.apenergy.2017.03.016**.

18 G. W. Taylor, J. R. Burns, S. Kammann, W. B. Powers and T. R. Welsh, The energy harvesting eel: a small subsurface ocean/river power generator, *IEEE J. Oceanic Eng.*, 2001, **26**(4), 539–547, DOI: **10.1109/48.972090**.

19 D.-A. Wang and N.-Z. Liu, A shear mode piezoelectric energy harvester based on a pressurized water flow, *Sens. Actuators, A*, 2011, **167**(2), 449–458, DOI: **10.1016/j.sna.2011.03.003**.

20 K. Fan, Z. Liu, H. Liu, L. Wang, Y. Zhu and B. Yu, Scavenging energy from human walking through a shoe-mounted piezoelectric harvester, *Appl. Phys. Lett.*, 2017, **110**(14), 143902, DOI: **10.1063/1.4979832**.

21 W.-S. Jung, M.-J. Lee, M.-G. Kang, H. G. Moon, S.-J. Yoon and S.-H. Baek, *et al.*, Powerful curved piezoelectric generator for wearable applications, *Nano Energy*, 2015, **13**, 174–181, DOI: **10.1016/j.nanoen.2015.01.051**.

22 K.-B. Kim, W. Jang, J. Y. Cho, S. B. Woo, D. H. Jeon and J. H. Ahn, *et al.*, Transparent and flexible piezoelectric sensor for detecting human movement with a boron nitride nanosheet (BNNS), *Nano Energy*, 2018, **54**, 91–98, DOI: **10.1016/j.nanoen.2018.09.056**.

23 A. C. Turkmen and C. Celik, Energy harvesting with the piezoelectric material integrated shoe, *Energy*, 2018, **150**, 556–564, DOI: **10.1016/j.energy.2017.12.159**.

24 A review of walking energy harvesting using piezoelectric materials, *IOP Conference Series: Materials Science and Engineering*, ed. E. M. Nia, N. A. W. A. Zawawi and B. S. M. Singh, IOP Publishing, 2017, DOI: **10.1088/1757-899X/291/1/012026**.

25 M. Zhu, E. Worthington and J. Njuguna, Analyses of power output of piezoelectric energy-harvesting devices directly connected to a load resistor using a coupled piezoelectric-circuit finite element method, *IEEE Trans. Ultrason. Ferroelectr. Freq. Control*, 2009, **56**(7), 1309–1317.

26 S. Sun, Y. Fang, G. Kieslich, T. J. White and A. K. Cheetham, Mechanical properties of organic–inorganic halide perovskites, CH 3 NH 3 PbX 3 (X= I, Br and Cl), by nanoindentation, *J. Mater. Chem. A*, 2015, **3**(36), 18450–18455, DOI: **10.1039/C5TA03331D**.

27 Y. Rakita, S. R. Cohen, N. K. Kedem, G. Hodes and D. Cahen, Mechanical properties of APbX3 (A= Cs or CH3NH3; X= I or Br) perovskite single crystals, *MRS Commun.*, 2015, **5**(4), 623–629, DOI: **10.1557/mrc.2015.69**.

28 Q. Tu, I. Spanopoulos, E. S. Vasileiadou, X. Li, M. G. Kanatzidis and G. S. Shekhawat, *et al.*, Exploring the factors affecting the mechanical properties of 2D hybrid organic–inorganic perovskites, *ACS Appl. Mater. Interfaces*, 2020, **12**(18), 20440–20447, DOI: **10.1021/acsami.0c02313**.

29 W. Wei, H. Gao, X. Lei, G. Feng and W. Li, Synthesis and mechanical properties of a new 1D hybrid organic-inorganic lead iodide, *Inorg. Chem. Commun.*, 2017, **85**, 45–48, DOI: **10.1016/j.inoche.2017.05.026**.

30 M. Kiran, S. Varughese, C. M. Reddy, U. Ramamurty and G. R. Desiraju, Mechanical anisotropy in crystalline saccharin: nanoindentation studies, *Cryst. Growth Des.*, 2010, **10**(10), 4650–4655, DOI: **10.1021/cg1009362**.

31 B. P. Gabriele, C. J. Williams, M. E. Lauer, B. Derby and A. J. Cruz-Cabeza, Nanoindentation of molecular crystals: Lessons learned from aspirin, *Cryst. Growth Des.*, 2020, **20**(9), 5956–5966, DOI: **10.1021/acs.cgd.0c00635**.

32 R. Devarapalli, S. B. Kadambi, C.-T. Chen, G. R. Krishna, B. R. Kammari and M. J. Buehler, Remarkably distinct mechanical flexibility in three structurally similar semiconducting organic crystals studied by nanoindentation and molecular dynamics, *Chem. Mater.*, 2019, **31**(4), 1391–1402, DOI: **10.1021/acs.chemmater.8b04800**.

33 W. M. Awad, D. W. Davies, D. Kitagawa, J. M. Halabi, M. B. Al-Handawi and I. Tahir, *et al.*, Mechanical properties and peculiarities of molecular crystals, *Chem. Soc. Rev.*, 2023, **52**(9), 3098–3169, DOI: **10.1039/D2CS00481J**.

34 J. Li, Y. Zhu, P. Z. Huang, D. W. Fu, Q. Q. Jia and H. F. Lu, Ferroelasticity in organic–inorganic hybrid perovskites, *Chem. – Eur. J.*, 2022, **28**(59), e202201005, DOI: **10.1002/chem.202201005**.

35 M. J. Turner, S. P. Thomas, M. W. Shi, D. Jayatilaka and M. A. Spackman, Energy frameworks: insights into interaction anisotropy and the mechanical properties of molecular crystals, *Chem. Commun.*, 2015, **51**(18), 3735–3738, DOI: **10.1039/C4CC09074H**.

36 W. C. Oliver and G. M. Pharr, An improved technique for determining hardness and elastic modulus using load and displacement sensing indentation experiments, *J. Mater. Res.*, 1992, **7**(6), 1564–1583, DOI: **10.1557/JMR.1992.1564**.

37 M. A. Reyes-Martinez, A. L. Abdelhady, M. I. Saidaminov, D. Y. Chung, O. M. Bakr and M. G. Kanatzidis, *et al.*, Time-Dependent Mechanical Response of APbX3 (A= Cs, CH3NH3;

X= I, Br) Single Crystals, *Adv. Mater.*, 2017, **29**(24), 1606556, DOI: **10.1002/adma.201606556**.

38 Q. Tu, I. Spanopoulos, S. Hao, C. Wolverton, M. G. Kanatzidis and G. S. Shekhawat, *et al.*, Out-of-plane mechanical properties of 2D hybrid organic–inorganic perovskites by nanoindentation, *ACS Appl. Mater. Interfaces*, 2018, **10**(26), 22167–22173.

39 J. C. Tan and A. K. Cheetham, Mechanical properties of hybrid inorganic–organic framework materials: establishing fundamental structure–property relationships, *Chem. Soc. Rev.*, 2011, **40**(2), 1059–1080.

40 T. L. Cottrell, The Strengths of Chemical Bonds, (No Title), 1954.

41 D. P. Karothu, J. Mahmoud Halabi, E. Ahmed, R. Ferreira, P. R. Spackman and M. A. Spackman, *et al.*, Global analysis of the mechanical properties of organic crystals, *Angew. Chem., Int. Ed.*, 2022, **61**(10), e202113988, DOI: **10.1002/anie.202113988**.